

Luminescent

40. Luminescent Materials

This chapter surveys the field of solid-state luminescent materials, beginning with a discussion of the different ways in which luminescence can be excited. The internal energy-level structures of luminescent ions and centres, particularly rare-earth ions, are then discussed before the effects of the vibrating host lattice are included. Having set the theoretical framework in place, the chapter then proceeds to discuss the specific excitation process for photo-stimulated luminescence and thermally stimulated luminescence before concluding by surveying current applications, including plasma television screens, long-term persistent phosphors, X-ray storage phosphors, scintillators, and phosphors for white LEDs.

40.1	Luminescent Centres	985	40.1.3	s^2 Ions	987
	40.1.1 Rare-Earth Ions	985	40.1.4	Semiconductors	987
	40.1.2 Transition-Metal Ions	986	40.2	Interaction with the Lattice	987
			40.3	Thermally Stimulated Luminescence	989
			40.4	Optically (Photo-)Stimulated Luminescence	990
			40.5	Experimental Techniques – Photoluminescence	991
			40.6	Applications	992
			40.6.1	White Light-Emitting Diodes (LEDs)	992
			40.6.2	Long-Persistence Phosphors	992
			40.6.3	X-Ray Storage Phosphors	993
			40.6.4	Phosphors for Optical Displays	994
			40.6.5	Scintillators	994
			40.7	Representative Phosphors	995
			References		995

Luminescent materials are substances which convert an incident energy input into the emission of electromagnetic waves in the ultraviolet (UV), visible or infrared regions of the spectrum, over and above that due to

black-body emission. A wide range of energy sources can stimulate luminescence, and their diversity provides a convenient classification scheme for luminescence phenomena, which is summarised in Table 40.1. Pho-

Table 40.1 Types of luminescence

Designation	Excitation	Trigger	Acronym
Photoluminescence	UV, visible photons	–	PL
Radioluminescence	X-ray, gamma rays, charged particles	–	RL
Cathodoluminescence	Energetic electrons	–	CL
Electroluminescence	Electric field	–	EL
Thermoluminescence	Photons, charged particles	Heat	TSL
Optically/photo-stimulated luminescence	Photons, charged particles	Visible/IR photons	OSL, PSL

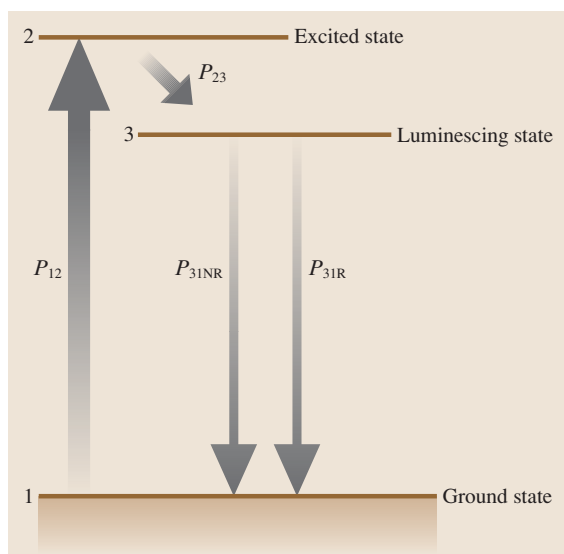


Fig. 40.1 Optical pumping cycle for a generic photoluminescent system

toluminescence, where the luminescence is stimulated by UV or visible light, is a widely used materials science technique for characterising dopants and impurities, and finds applications in lighting technologies such as fluorescent lamps. Radioluminescence involves excitation by ionising radiation, and is used in scintillators for nuclear particle detection; the special case of stimulation by energetic electrons is called cathodoluminescence, the name arising from early atomic physics experiments involving gas discharges. The major application of cathodoluminescence is in cathode ray tubes for television sets and computer monitors. Electroluminescence involves collisional excitation by internal electrons accelerated by an applied electric field, and with a much lower energy than in the case of cathodoluminescence. Electroluminescence finds applications in panel lighting used in liquid-crystal display (LCD) back-planes, and in light-emitting diodes.

There are other forms of luminescence which we mention for completeness but will not discuss further: bioluminescence and chemiluminescence where the energy input is from chemical or biochemical reactions, sonoluminescence (sound wave excitation), and triboluminescence (strain or fracture excitation).

There are several books which describe the luminescence of materials in more depth than is possible in a short article, for example that edited by Vij [40.1] and the monograph by Blasse and Grabmaier [40.2].

The terms phosphorescence and fluorescence are often used in connection with luminescent materials. This classification is based on the time-domain response of the luminescent system. Figure 40.1 shows a generic photoluminescent system where incident UV radiation excites a system from a ground state 1 with probability per unit time P_{12} into an excited state 2. The system decays with probability P_{23} to a luminescing level 3, from which there is a probability P_{31R} and P_{31NR} of radiative and nonradiative decay, respectively, to the ground state. Nonradiative decay generally involves phonon emission.

First suppose that the transition probabilities are such that $P_{12}, P_{21} \gg P_{31} (= P_{31R} + P_{31NR})$. If the optical pumping (excitation) is abruptly stopped, the population of the luminescing state 3 decays as,

$$N_3 = N_3(0) \exp(-P_{31}t) \quad (40.1)$$

and the rate of luminescent energy emission is $-(h\nu P_{31R}/P_{31}) dN_3/dt$ for an energy difference $E_{31} = h\nu$ between states 1 and 3. Hence the luminescence intensity at distance r from the sample is,

$$I = (h\nu) N_3(0) P_{31R} \exp(-P_{31}t) / (4\pi r^2) \quad (40.2)$$

and the characteristic luminescence lifetime is $\tau = (P_{31})^{-1}$. Thus the lifetime is governed by both radiative and nonradiative processes, whilst the intensity of the luminescence depends on the relative magnitude of P_{31R} .

This discussion provides the basis for understanding the terms fluorescence and phosphorescence applied to luminescent materials. A material is often classified as one or the other according to the relative magnitude of $\tau = (P_{31})^{-1}$, with 10 ns being set in a relatively arbitrary way as the boundary between a *fast* fluorescent system and a *slow* phosphorescent one. For comparison, the theoretical lifetime for spontaneous emission for a strongly allowed hydrogen atom $2p \rightarrow 1s$ transition is about 0.2 ns.

However, by this definition phosphorescence can also arise from luminescent states with short lifetimes which are populated through ones with long lifetimes. In Fig. 40.1, if state 2 is long-lived in the sense that $P_{23} \ll P_{31}$ then the measured lifetime for emission from the luminescing state will be $\tau = (P_{23})^{-1}$, and the system will be labelled phosphorescent, even though the luminescing level itself has a very short lifetime. In consequence, a second classification [40.2] is based on whether or not the luminescing level is fed by a metastable state which sets the lifetime. Sometimes the metastable state is a long-lived intermediate form

of energy storage which can be triggered by an external stimulus to undergo a transition to a fluorescent level. Thus in Table 40.1, thermally stimulated and optically stimulated luminescence involve a metastable state consisting of trapped electrons and holes, which can be triggered to recombine by heating or by optical

stimulation; the recombination energy is transferred to a fluorescing centre.

Overall, the fluorescence/phosphorescence classification is somewhat nebulous, and it is debatable whether the classification is necessary or desirable.

40.1 Luminescent Centres

A wide variety of centres give rise to luminescence in semiconductors and insulating materials, including rare-earth ions, transition-metal ions, excitons, donor–acceptor pairs, and ions with a d^{10} or s^2 electronic configuration ground state. Some luminescence spectra consist of broad emission bands arising from the interaction between the electronic system of the luminescent centre and the vibrations of the atoms or ions, which surround it; the broad bands arise from simultaneous transitions of both electronic and vibrational systems. For others, such as the rare earths, the spectra comprise sharp lines arising from purely electronic transitions, and the effect of the environment is felt mainly through their effects on the lifetimes of the states. Thus in discussing the physical background to luminescence, it is simplest to start with a discussion of rare-earth luminescence, where the effect of vibrations can be initially ignored.

40.1.1 Rare-Earth Ions

The trivalent rare-earth ions have n electrons ($n = 1 - 14$) in the $4f$ shell. In a free ion, the eigenstates resulting from the various atomic interactions are labelled by the total spin S and orbital angular momenta L . Spin–orbit coupling breaks up each L, S multiplet of degeneracy $(2S + 1)(2L + 1)$ into sub-multiplets labelled by the total angular momentum $J = L + S$, where J can range from $L - S$ to $L + S$. The $4f^n$ orbitals lie within the outer $5s^2$ and $5p^6$ filled shells, which partly shield them from the effects of a crystalline environment. The effects of the latter are quantitatively described by the *crystal field* [40.3], and this term in the Hamiltonian splits the J multiplets into $2J + 1$ sublevels, the so-called crystal-field splitting. Some of these crystal-field levels may still be two- or threefold degenerate, depending upon the symmetry of the environment. Odd-electron systems always have at least twofold (Kramers) degeneracy. The resulting energy-level structures are complicated, and are summarised in the classic *Dieke di-*

agram [40.3]. The original has been updated by *Carnall et al.* [40.4] and is reproduced in many books and papers on rare-earth ion spectroscopy [40.2]. In Fig. 40.2, we show a schematic version (not accurately to scale) of the diagram appropriate for Pr^{3+} with $n = 2$, which serves for our discussion. The crystal-field splitting is usually smaller than the spin–orbit splitting, and is illustrated schematically by the vertical extent of the bands in Fig. 40.2. The multiplet labels follow the usual $^{2S+1}L_J$ system.

In the figure we also show a generic highest excited band which does not belong to the $4f^2$ configuration. In the specific case of the rare earths this can be the excited-state configuration resulting from promo-

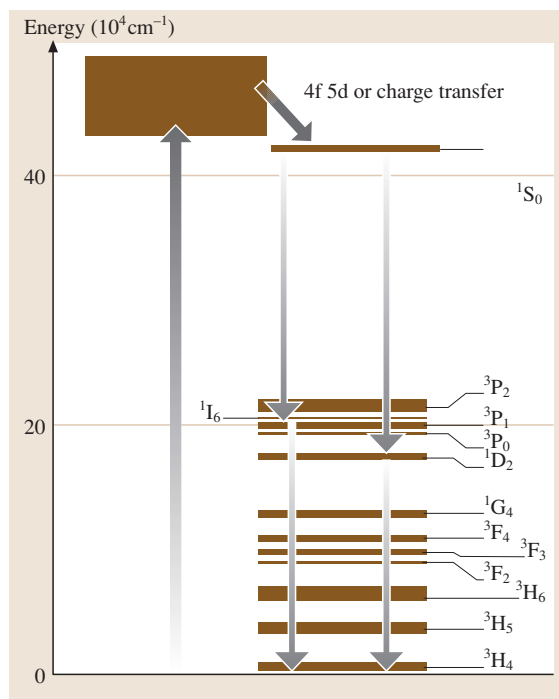


Fig. 40.2 Schematic energy-level diagram for Pr^{3+}

tion of one electron to the 5d state, giving an overall $4f^{n-1}5d^1$ configuration; more generally it could be a so-called charge transfer band, which corresponds to the transfer of one electron from the ligands to the luminescent ion. The relative location and importance of these bands varies with the luminescent ion and the crystalline environment, but they play an important role in the excitation of luminescence.

Excitation and luminescence transitions within the various levels in Fig. 40.2 are governed by the golden rule of quantum mechanics [40.5] for interactions with the electromagnetic field; in summary the probability of a transition between two states i and j is proportional to square of the matrix element $\langle i|H|j\rangle$, where H is the time-dependent perturbation Hamiltonian representing the interaction of the electrons with the electromagnetic field. The proportionality constant contains the light intensity in the case of excitation. The perturbation can be expanded in a power series involving electric and magnetic multipoles of the electronic system, but of these the electric dipole term is dominant, with the magnetic dipole term being much smaller by a factor of more than five orders of magnitude. Since the electric dipole operator $e\mathbf{r}$ has odd parity, the matrix element for transitions $r_{ij} = \langle i|e\mathbf{r}|j\rangle$ is necessarily zero unless i and j have opposite parity. This is the most important selection rule governing luminescence: transitions between states of the same parity have zero transition probability and so are *forbidden* (Laporte's rule). In the case of the rare earths, all states of a single $4f^n$ configuration have the same parity, and so all optical transitions within the configuration are strictly forbidden. But this rule is relaxed by several considerations. First, if the crystalline environment lacks inversion symmetry, the crystal field admixes a small fraction of the excited configurations (eg $4f^15d^1$ for Pr^{3+}) of opposite parity into the ground configuration, which makes such transitions weakly allowed. Secondly, the selection rule for magnetic dipole transitions is that they are allowed between states of the same parity, although they are typically about five orders of magnitude weaker than for electric dipole ones. Finally, odd-parity vibrations and an electron-phonon interaction produce a similar configuration admixture effect to static lattice odd-parity mixing although this effect is more important for 3d ions than for 4f ones.

With only weak transitions possible within the 4f configuration, one might wonder how it would be possible to optically excite any significant luminescence. The answer lies in the 5d or charge-transfer bands which either lie at higher energies, or overlap with the upper levels of the 4f configuration. These give rise to strong

absorption and efficient pumping. Relaxation can occur via the parity-allowed transitions to the upper levels of the 4f configuration, and from there via single or multiple radiative emissions back to the ground state. Because these intra-configurational transitions are only weakly allowed, the lifetimes are generally quite long, of the order of μs – ms . Figure 40.2 shows some of the observed transitions in the case of the Pr^{3+} ion. There are further constraints on possible transitions which arise from an analysis of the angular momenta of the initial and final states. For example, a transition between two states both of which have $J = 0$ is forbidden since there is no angular momentum change as required for a photon; similarly for dipole transitions we require $\Delta J = 0, \pm 1$.

The transition probability per second for spontaneous emission [40.6] is given by

$$P_{ij} = \frac{64\pi^4\nu^3}{3hc^3} |r_{ij}|^2, \quad (40.3)$$

where ν is the frequency of the transition, h is Planck's constant, c is the velocity of light, and $|r_{ij}|$ is the matrix element of the electric dipole operator $e\mathbf{r}_{ij}$ between the two states i and j , and e is the electronic charge. For absorption, this must be multiplied by N , the mean number of photons with energy $h\nu$, which thus incorporates the effect of the incident beam intensity. Experimentally, one measures an absorption coefficient k as a function of energy $k(E)$ [40.6] which is linked to P_{ij} through,

$$\int k(E)dE = N_i \left(\frac{\pi e^2 h}{nmc} \right) \left(\frac{n^2 + 2}{3} \right)^2 f_{ij}, \quad (40.4)$$

where n is the refractive index of the crystal environment, m is the electronic mass, N_i is the concentration of the luminescent centres, and f is the *oscillator strength* for the transition. For both absorption and emission, the dimensionless oscillator strength f_{ij} defined as [40.6]

$$f_{ij} = \frac{8\pi^2 m \nu}{3h e^2} |r_{ij}|^2 \quad (40.5)$$

is often quoted to compare the relative transition probabilities. For an electron harmonic oscillator, $\sum f_{ij} = 1$, and so oscillator strengths of the order of 0.1–1 are strongly allowed transitions.

40.1.2 Transition-Metal Ions

Transition-metal ions from the 3d series are characterised by a much stronger interaction with the crystalline environment than the 4f ions since there is no equivalent of screening by the 5s, 5p outer shells. In addition, the spin-orbit coupling is weaker, and so the order

of perturbation is reversed: the atomic L , S multiplets are split by the crystal field, with spin-orbit coupling being a smaller interaction. Intra-configurational transitions are again strictly forbidden, but become weakly allowed by inter-configurational mixing through odd-parity crystal fields, and by odd-parity vibrations. The result of this is that the strongest selection rule after parity is that transitions should have $\Delta S = 0$, since the electric dipole operator does not involve spin. The other major difference, again due to the strength of the crystal-field interaction, is that transitions which are purely electronic, the so-called zero-phonon lines, are rarely observed. Rather what are seen are broad bands which correspond to the simultaneous excitation of an electronic transition and vibrational transitions, which overlap to give the broad observed bands. In particular, transitions involving odd-parity vibrations have a high transition probability through the effect of configuration admixing. This will be considered in a following section. The most commonly observed luminescent ions are those from the d^3 configuration (Cr^{3+} , Mn^{4+}) and from the d^5 configuration (Mn^{2+}).

40.1.3 s^2 Ions

The $5s^2$ (e.g. Sn^{2+} and Sb^{3+}) ions and $6s^2$ (e.g. Tl^+ , Pb^{2+} , Bi^{3+}) ions are of considerable importance because transitions to and from the excited s^1p^1 states are Laporte-allowed. The interaction of the p state with the

crystalline environment can be very strong, and so broad spectra are often observed.

40.1.4 Semiconductors

Luminescence in semiconductors is dominated by near-band-gap luminescence arising from recombination of electrons and holes. This process is most efficient in direct-band-gap materials such as ZnS and GaP rather than indirect-band-gap materials such as Si and Ge because the transition probability requires conservation of wavevector, but the photon wavevector is ≈ 0 on the scale of the Brillouin zone. Hence creation or destruction of a phonon is required for band-to-band luminescence in indirect-gap materials, which is less probable. The near-edge emission may correspond to luminescence from a variety of shallow energy-level structures such as free or trapped excitons, or from donor-acceptor recombination. These are both examples of electronic systems with spatially extensive wavefunctions, in contrast to the atomically localised $3d$ and $4f$ wavefunctions considered earlier. However, it is also possible to observe *deep-level* luminescence from transition-metal ions and rare earths in semiconductors provided that the electron affinities and band-gap energies are such that the pertinent energy levels fall in the band gap. Since semiconductors are discussed elsewhere in this volume, we shall not consider them further here.

40.2 Interaction with the Lattice

For rare-earth ions, the interaction with the vibrations of the crystal lattice can be ignored for most purposes; the observed luminescence spectrum consists of sets of sharp electronic transitions. But for other luminescent ions which interact strongly with the vibrating ions of the surrounding crystal, the incorporation of the latter is critical to explaining the observed spectra. The simplest model of ion-lattice interactions is to consider only the N nearest neighbour ions and their atomic displacements X_n , Y_n , Z_n , ($n = 1, N$) in Cartesian coordinates. The vibrational Hamiltonian involves cross terms in these coordinates, but may be transformed to harmonic form if symmetry-adapted forms of these coordinates (*normal modes*) are used instead of the actual displacements. For example, the so-called breathing mode Q_b , for an octahedrally coordinated ion takes the form

$$Q_b = (Z_1 - Z_2 + X_3 - X_4 + Y_5 - Y_6)/6. \quad (40.6)$$

If all the other modes have zero amplitude, the ions move radially towards or away from the central luminescent ion. The key point in considering the influence of the crystal lattice is that the vibrational potential energy is just the variation of the electronic energy with ionic displacement, or equivalently with the normal modes (within the spirit of the Born-Oppenheimer approximation). Put another way, the crystal field depends on the ion positions so that the electron and lattice quantum-mechanical systems are linked through this electron-lattice coupling. We can therefore expect a difference in the harmonic vibrational potential from one electronic state to another, so that it will in general have the form $(1/2)m\omega_i^2(Q - Q_{0i})^2$; i.e. both the magnitude of the potential and the position of the minima Q_{0i} will depend on the electronic state i . The vibrational states in the harmonic approximation are just the usual simple harmonic oscillator states with energies $(n + 1/2)h\nu_i$,

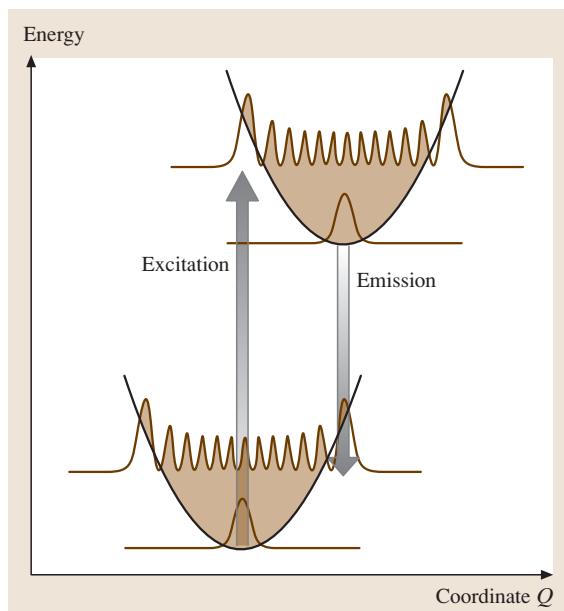


Fig. 40.3 Configuration coordinate diagram for excitation/emission cycle

with n an integer. Thus we arrive at a *configuration coordinate* diagram such as that shown in Fig. 40.3, with the potential energies for a ground state g and excited state e being offset parabolas of different curvature. The square of the vibrational wavefunction is shown for the ground state and that with $n = 11$. We note that for a classical oscillator there would be a peak in the probability function at the extreme lengths of travel, corresponding to the maxima for $n = 11$ at the outer limits of the wavefunction in Fig. 40.3.

We consider first luminescence from the excited electronic state/lowest vibrational state. The transition probability may be calculated using the Franck–Condon principle, that is we assume that the duration of the electronic transition is much shorter than a vibrational period, so that the Q remains constant during a transition. The transition is therefore taken to be *vertical* on the configuration coordinate diagram. The transition probability is just $\langle \phi_e | \phi_g \rangle^2$, the square of the vibrational wavefunction overlap, multiplied by the electronic transition probability considered earlier. From Fig. 40.3, this overlap will be a maximum for some vibrational state other than the ground state, unless the positions of the minima of the two potential energy curves coincide accidentally. (In Fig. 40.3, this maximum would be for the $n = 11$ ground vibrational state). Put another way, the maximum transition probability is not

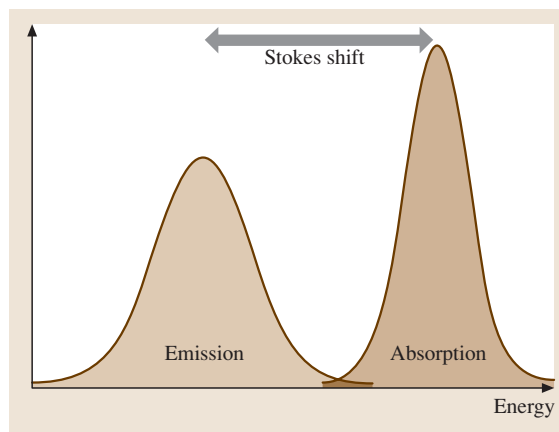


Fig. 40.4 Absorption and emission line shapes for strong electron–lattice coupling

for the zero-phonon transition (no change in vibrational state), but corresponds to the creation of a finite number of phonons. A range of transitions is allowed, and the result in a semiclassical analysis, allowing for finite line widths, is a Gaussian-shaped band. The analysis has to be extended to include finite temperatures and other modes, but the overall result is that the emission line shape is approximately a Gaussian centred at an energy lower than that of the difference between the minima of the two potential curves. The same argument can be applied to the excitation process, and again an approximately Gaussian line shape results but this time centred on an energy above that of the difference in potential-energy minima. Figure 40.4 shows the overall result; the difference between the maxima of the two curves, known as the Stokes shift, is an indicator of the degree of electron–lattice coupling.

It is clear from the diagram that the, in cases where there is strong electron–lattice coupling of this type, that: (a) there will be very little intensity in the zero-phonon line, and (b) there will be a large Stokes shift between the energies for maximum absorption and maximum emission. Thus the luminescence of transition-metal ions, colour centres, and closed-shell ground-state ions (s^2 , d^0), which have strong interactions with the lattice in the excited states, are typically broad bands with only occasionally weak, sharp zero-phonon lines being observed. For luminescence from within the 4f states of the rare earths, the reverse is true; we are in the weak-coupling regime, and zero-phonon lines are the predominant features of the spectrum.

40.3 Thermally Stimulated Luminescence

Thermally stimulated luminescence (TSL), or simply thermoluminescence (TL), refers to luminescence induced by thermally stimulated recombination of trapped electrons and holes in materials which have been subject to prior irradiation. The irradiation, which may be in the form of UV light, X-rays, gamma rays, or energetic electrons, creates free electrons and holes, most of which promptly recombine, but some of which are locally trapped at defect centres such as impurities and vacancies. If the trap binding energies are sufficiently large, thermal promotion of the electron or hole to the conduction band or valence band, respectively, is improbable at the irradiation temperature, and so these charge carriers remain trapped after irradiation. However, if the sample is then heated, thermally assisted recombination becomes increasingly probable, and the result is an initially increasing light output with increasing temperature until the traps are depleted, whereupon the light intensity drops. The curve of light intensity versus temperature $I(T)$ is known as a glow curve, and may be analysed to extract the trap depths and concentrations. A comprehensive review of the field has been given by *McKeever* [40.7], and a shorter discussion is given by *Vij* [40.1].

The process is shown schematically for a simple system comprising a single electron trapping level T and a single recombination centre R in Fig. 40.5.

Irradiation results in a trapped electron at trap T and a trapped hole at R . The trapped hole binding energy is larger than that of the trapped electron, so the latter is depopulated first, with a probability P which has the form,

$$P = s \exp(-E/kT) , \quad (40.7)$$

where s and E are the attempt frequency and the activation energy respectively. We have shown the hole trap and recombination centre as being one and the same in Fig. 40.5, but it is also possible that the recombination energy is transferred to a separate luminescent centre.

In the measurement process, the sample is heated at a fast and linear rate, typically 1–10 K/s, whilst the light emission is monitored by a sensitive filter/photomultiplier combination, or by a monochromator system. The resulting glow curve may be fitted to a theoretical curve to extract the trap parameters. Generally the light output is quite weak, and TSL systems have sensitivity as one of their prime design factors, so cooled detectors and photon counting are commonplace. Above about 400 °C, thermal radiation from the sample/heater

is a problem and must be eliminated by filtering or by subtraction of a glow curve recorded using a thermally bleached sample.

The main uses of TSL are in determining trap depths and irradiation doses. In archaeological and geological applications, a comparison is made between accumulated natural dose and a dose from a radioisotope; by combining this with a measurement of the activity of the surroundings, a date since last thermal or optical erasure

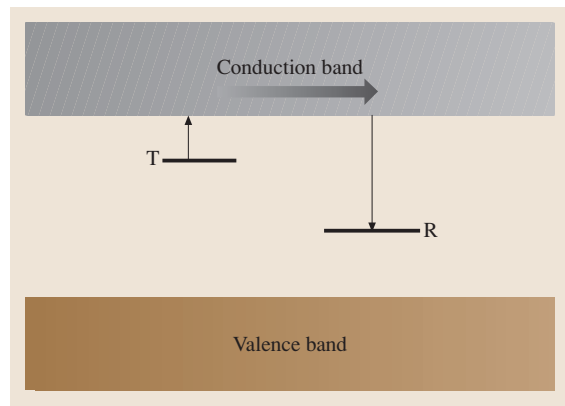


Fig. 40.5 Thermally stimulated luminescence process

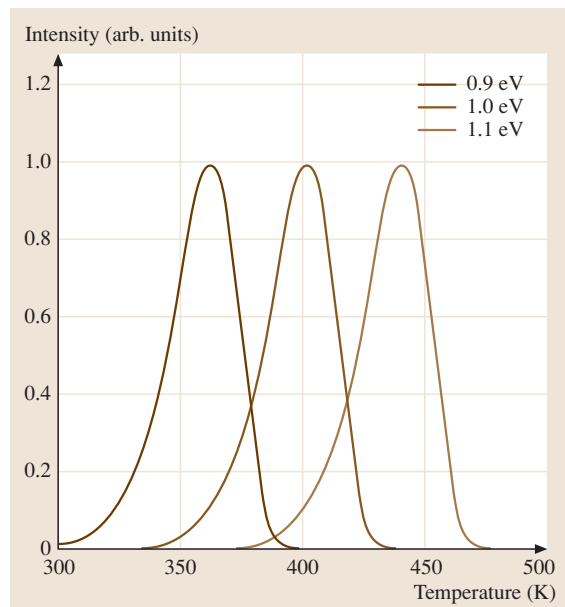


Fig. 40.6 Computed glow curves for first-order kinetics for fixed escape frequency and various trap depths

of the object can be determined. The nature of the traps is often poorly understood for these chemically complex samples. For medical dosimetry, room-temperature stable traps with high thermoluminescent output are required. At present, the material of choice is LiF doped with a few hundred ppm of Mg and Ti.

The mathematical form of the TSL glow curve depends on the physical model used for the TL process. In the simplest case, assuming first-order kinetics [40.1, 7], the light intensity I at temperature T is given by,

$$I(T) = n_0 s \exp(-E/k_B T) \times \exp \left[- (s/\beta) \int_{T_0}^T \exp(-E/k_B T) dT \right], \quad (40.8)$$

where n_0 is the number of occupied traps at time $t = t_0$ when the temperature is T_0 , β is the heating rate in K/s, and k_B is Boltzmann's constant. The result is a glow curve whose peak position varies approximately linearly with trap depth E , as shown in Fig. 40.6 (for fixed escaped frequency $s = 3.3 \times 10^{11} \text{ s}^{-1}$ and heating rate 1 K/s).

Of course, the peak position also depends on the escape frequency s , but is less sensitive to s than to E . For second-order kinetics [40.1, 7], the glow curve equation becomes

$$I(T) = \left(n_0^2 s / N \right) \exp(-E/k_B T) / \left[1 + (n_0 s / N \beta) \int_{T_0}^T \exp(-E/k_B T) dT \right]^2, \quad (40.9)$$

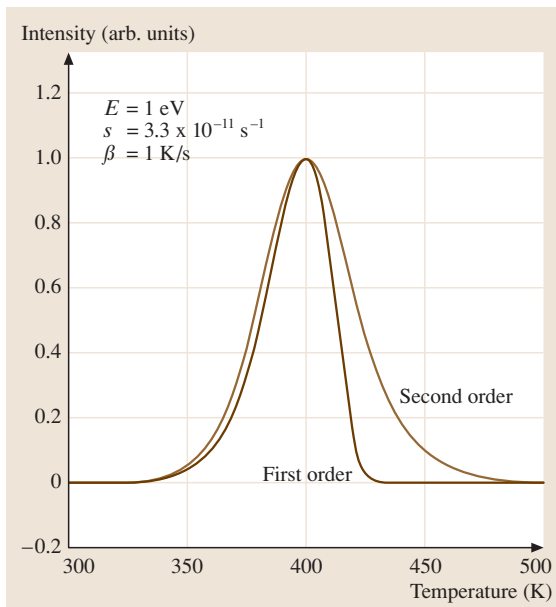


Fig. 40.7 Comparison of first- and second-order glow curves

where N is the number of available traps. The two forms both give glow curves of similar shape, but the first-order form shows an asymmetric form with a sharp fall off on the high-temperature side of the peak, whilst the second-order form is more symmetric as shown in Fig. 40.7. The parameters are extracted by least-squares fitting of these expressions to the experimental glow curves, which is cumbersome due to the integral, but *Kitis et al.* [40.8] have given analytical approximations to (40.8) and (40.9). In practice, many glow curves do not follow first- or second-order kinetics precisely.

40.4 Optically (Photo-)Stimulated Luminescence

Thermally stimulated luminescence is sometimes also accompanied by optically stimulated luminescence (OSL), in which one of the trapped carriers is excited by optical stimulation to a level from which it can recombine with the conjugate carrier by tunnelling, or completely to one of the bands so that recombination is achieved through what is essentially a photoconductivity effect. For OSL to be significant,

there must be an appreciable optical transition probability, so not all TSL centres are OSL active. The stimulation energy measured in OSL generally differs from that determined from TSL because of the Franck–Condon principle. The OSL effect finds practical application in dosimetry, e.g. [40.9], and in X-ray storage phosphors used for medical imaging, as described later.

40.5 Experimental Techniques – Photoluminescence

A typical traditional photoluminescence measuring system involves a broad-spectrum source, either a combined tungsten filament for the visible spectrum and deuterium lamp for the UV, or a xenon flash lamp. The lamp emission is passed through a grating monochromator and so selectively excites the luminescence. Band-pass or band-edge filters are generally required to eliminate unwanted second- and higher-order diffraction maxima from the grating. The luminescence is efficiently gathered by low- f /number optics and fed to a second grating monochromator, also equipped with filters, to monitor and analyse the luminescence. The final detector may be a photomultiplier, or preferably a charge-coupled device or photodiode array for improved data collection efficiency at multiple wavelengths.

This arrangement relies on good monochromatization/filtering to remove what is sometimes a relatively strong component of scattered light from the beam analysed by the emission monochromator. An alternative method of removing scattered light is to use time discrimination, by replacing the source by a xenon flash lamp (for example, as in the common Perkin Elmer LS55B luminescence spectrometer). The flash has a duration of about $10\ \mu\text{s}$, so any scattered light has decayed away to an insignificant level when the emitted beam is sampled some time ($0.1\text{--}10\ \text{ms}$) after the flash. A timed electronic gate is used to sample the emission immediately after a flash and just before the next flash; the difference between these two sampled signals gives the short-term luminescence whilst the second sample alone gives the long-term luminescence with *long* and *short* being relative to the flash repetition period. Of course, luminescence with lifetimes shorter than the pulse width ($\approx 10\ \mu\text{s}$) cannot be readily measured with this system. The luminescence intensity is normalised with respect to the excitation intensity by steering a sample of the excitation beam to a rhodamine dye cell which has a quantum efficiency of essentially unity for wavelengths below about $630\ \text{nm}$. The fluorescence from the dye is measured with a second photomultiplier.

To minimise the effect of scattered light, a conventional laser with its intrinsically narrow linewidth and high intensity is a very convenient replacement for a broad-spectrum lamp, but suffers from the disadvantage of a fixed wavelength. Typical lasers of interest are nitrogen (pulsed), argon (UV lines, or frequency-doubled visible lines), krypton, and the new

generations of GaN/GaInN blue/violet/UV laser diodes. For rare-earth spectroscopy, or other systems which are characterised by narrow absorption lines, it is very useful to have a scanning dye laser as the excitation source. This *selective excitation* facility enables *tagging* of particular luminescent levels with excited states belonging to the same centre, so that a picture of the energy-level structure of each luminescent centre can be built up in cases where several such centres contribute to the overall luminescence.

For decay kinetics on faster time scales, fluorimeters such as those developed initially by the Spex company (now Horiba) use a fast modulator and phase-sensitive detection to measure the phase shift between fluorescence and excitation; it is claimed that fluorescence decays can be measured with a resolution of $25\ \text{ps}$ this way. An alternative is the time-correlated single-photon-counting technique which can measure decay constants in the ps–ns range. In this method, the excitation comes from a fast laser pulse, and the light level reaching the photomultiplier or micro-channel plate detector is reduced to such a low level that less than one photon per excitation pulse is detected. The time delay between the photon detection and the time of the pulse is measured, and a histogram produced of numbers of detected photons versus arrival time taken over a large number of excitation pulses. For efficient data collection, a high repetition rate and fast-pulse laser are required, often a Ti–sapphire laser. The wavelength for Ti–sapphire is too large for stimulating many materials directly with single-photon excitation, but stimulation is nonetheless possible by a two-photon excitation process, or by the use of a nonlinear crystal acting as a frequency doubler to produce laser output at one half the wavelength of the basic laser.

There are a number of specialist techniques, such as hole-burning, fluorescence line-narrowing, and photon echo methods associated with the use of lasers with either very narrow line widths or short pulse duration which have developed in a parallel way to techniques first introduced in nuclear magnetic resonance, and which are mainly used to investigate the dynamics and quantum mechanics of the luminescent species rather than the material in which they are contained. *Meijerink* gives a review of experimental luminescence techniques [40.1] which includes a short discussion of these specialist techniques.

40.6 Applications

The largest market for luminescent materials has traditionally been in the areas of lighting, through fluorescent tubes, and in cathode-ray-tube screen phosphors for image display. Both of these areas can now be regarded as mature in terms of materials development. However, new discoveries in the past decade, and the advent of new technologies, have rekindled interest in phosphor materials. Some of the current areas of activity in applications are outlined below.

40.6.1 White Light-Emitting Diodes (LEDs)

The development of blue, violet and UV LEDs based on GaN, InGaN and other semiconductors and alloys has stimulated great interest in the possibility of producing a *white-light LED* for use in lighting applications. LEDs are now available with emissions which peak as low as 365 nm in the ultraviolet. The concept is to use the blue emission to stimulate luminescence from yellow, or red and green phosphors, so that when mixed with residual blue light from the LED the result is simulated white light. For UV LEDs the LED output is used to stimulate blue, red and green phosphors.

The first generation of white LEDs from companies such as Nichia relied on a YAG:Ce phosphor to convert

some of the emission from a 465-nm GaInN LED into an orange/yellow emission centred at 550 nm; the combination of blue and yellow simulates white light. More recent versions of this scheme include $\text{Sr}_3\text{SiO}_5:\text{Eu}^{2+}$, which emits at 570 nm, and is claimed [40.10] to be more efficient than YAG:Ce, and a CaSiAlON:Eu ceramic phosphor which offers improved thermal stability [40.11]. Improved colour rendition is obtained by using more phosphors and better balance between the various emissions, for example by replacing the YAG:Ce with $\text{SrGa}_2\text{S}_4:\text{Eu}$ (green) and $\text{SrY}_2\text{S}_4:\text{Eu}$ (red). Most recent developments based on 375 nm UV LEDs have used multiple emissions to achieve even better colour balance; for example Kim et al. [40.12] use $\text{Sr}_3\text{MgSi}_2\text{O}_8:\text{Eu}^{2+}$, Mn^{2+} , which has blue (Eu^{2+}), yellow (Eu^{2+}) and red emissions (Mn^{2+}).

A second development in this area is the substitution of another semiconductor for the phosphor – the so-called photon recycling technique. In this method, a layer of AlGaInP is used to absorb some of the blue incident radiation and down-convert it to the complementary colour. The advantage is that the fabrication/integration process is simpler compared to combining phosphor and semiconductor technology.

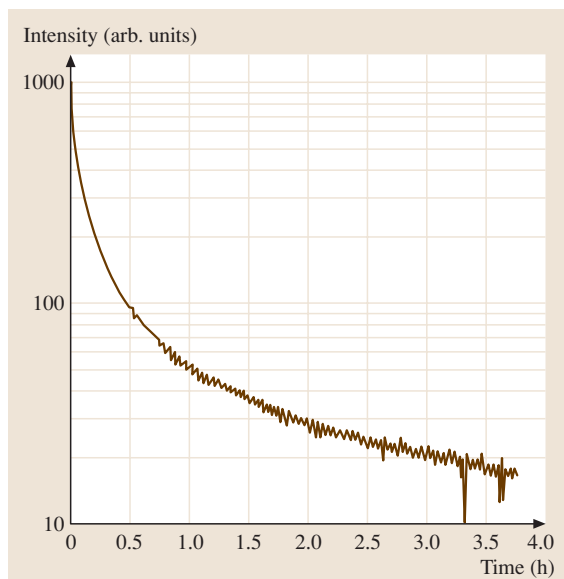


Fig. 40.8 Dark decay of persistent luminescence in a commercial lighting strip based on Nemoto $\text{SrAl}_2\text{O}_4:\text{Eu}/\text{Dy}$ material

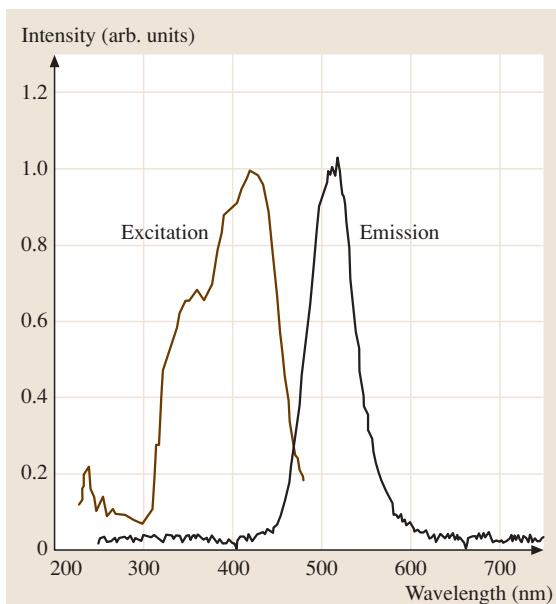


Fig. 40.9 Excitation and emission spectra of a commercial lighting strip based on Nemoto $\text{SrAl}_2\text{O}_4:\text{Eu}/\text{Dy}$ material

40.6.2 Long-Persistence Phosphors

It has been discovered in the past decade that some materials show a very long-lived but intense afterglow, arising from thermal emission of charge carriers from deep traps, followed by electron–hole recombination at or near a luminescent ion, i.e. room-temperature thermoluminescence. The persistence is for periods of several hours, much longer than the well-known ZnS:Cu persistent phosphor. This new class of materials have widespread applications in areas such as signage and passive emergency lighting for public buildings, aircraft cabins etc. The material is activated or *charged* by the blue/UV content of solar radiation or fluorescent indoor lighting during normal conditions; in subsequent dark conditions the energy is released as an afterglow. No power supply is required, the operation is entirely passive, and so a high degree of reliability is assured. Generally the phosphor powder ($\approx 10\ \mu$ grain size) is mixed with a resin binder and applied as a thick ($\approx 1\ \text{mm}$) coating. The materials which have been used are rare-earth-doped strontium or calcium aluminate [CaAl_2O_4 :Eu/Nd (blue), SrAl_2O_4 :Eu/Dy (green), $\text{Sr}_4\text{Al}_{14}\text{O}_{25}$:Eu/Dy (blue–green), and $\text{Y}_2\text{O}_2\text{S}$:Eu/Mg/Ti (orange)]. Figures 40.8 and 40.9 show the decay and emission/excitation characteristics of a commercial phosphor strip of this type, based on Luminova[®] SrAl_2O_4 :Eu/Dy powder sourced from the Nemoto company. The decay is clearly non–exponential, but after the initial rapid decay the intensity may be fitted with an exponential with a decay constant of 3.1 h.

The traps which are responsible for the long-lived decays in these systems have not been clearly identified, and it is likely that there are several involved. Jia et al. [40.13, 14] have studied persistent violet/UV and blue ($\approx 400\ \text{nm}$, $450\ \text{nm}$) luminescence from rare-earth ions in CaAl_2O_4 and BaAl_2O_4 and report that the thermally stimulated luminescence from these materials contains multiple glow peaks. They also describe how co-doping the calcium aluminate with Tb^{3+} results in a green persistent phosphor as a result of energy transfer from the cerium to the terbium ion; this mechanism could be the basis for convenient colour control, including white persistent phosphors. Aitasalo et al. [40.15] report that the nature of the traps is affected by the particular rare-earth ion or couple.

40.6.3 X-Ray Storage Phosphors

Optically stimulated or photo-stimulated luminescence is the basis for an X-ray imaging technology known

commercially as computed radiography (CR). CR was the first of a number of imaging techniques which are steadily replacing traditional photographic film methods. Several other techniques such as those based on amorphous selenium photoconductor/flat panels and a-Si arrays, and scintillator CCD/complementary metal–oxide–semiconductor (CMOS) arrays have also emerged in recent years, but CR is still the dominant of the new technologies on the basis of numbers of installed units. The many advantages of CR over photographic film, and the principles of the method are detailed in [40.16, 17], but the basic mechanism is that incident X-rays create electron–hole pairs in the material. Most of these promptly recombine, but some are trapped at defects and impurities, and remain trapped for periods of hours after the X-ray source is turned off. In an X-ray storage phosphor (XRSP), one of the trapped carriers is optically stimutable, and can be excited to the conduction band or valence band, or to a level from which it can recombine by tunnelling with the conjugate trapped carrier. The resulting recombination energy is transferred to a luminescent ion, and the intensity of the photo-stimulated luminescence (PSL) is in direct proportion to the incident X-ray intensity. The dominant material used in current XRSP systems is $\text{BaFBr}_{1-x}\text{I}_x$: Eu^{2+} , where the electron traps are F-centres, the hole traps are unidentified, and the luminescence is the $5d-4f$ transition of the Eu^{2+} ion. One disadvantage of systems based on this (powder) phosphor is that when the image is extracted with a raster-scanned He–Ne laser beam, light scattering from the powder grains means that material outside the focussed laser spot is also stimulated, limiting the spatial resolution to around $200\ \mu\text{m}$, which is inadequate for applications such as mammography. Several ways to overcome this are currently under development. $\text{RbBr}:\text{Eu}$ is also an X-ray storage phosphor [40.18] and can be grown by vapour deposition in a columnar form.

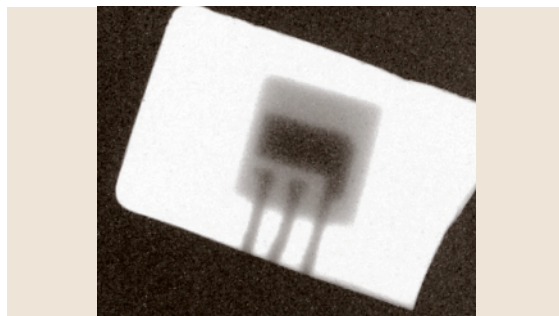


Fig. 40.10 PSL image of a BC549 transistor recorded on a glass-ceramic imaging plate

The columnar structure has a light-guiding property, restricting the scattering effect, and improving the resolution. A second development is that of glass-ceramic storage phosphors, where PSL active crystals are embedded in a glass [40.19–21]; the combination of particle size, separation and refractive-index mismatch means that these composite materials are semitransparent and the problem of scattering of read-out light is reduced. Figure 40.10 shows an image of a BC549 transistor recorded in a glass-ceramic X-ray storage phosphor.

40.6.4 Phosphors for Optical Displays

There are several new technologies being developed to replace cathode ray tubes for domestic televisions, including plasma display panels (PDPs). In these units, each pixel is a sealed cell containing a mixture of Xe and Ne in a dielectric-shielded electrode structure (for a review, see *Boeuf* [40.22]). An alternating current (AC) voltage applied between the electrodes results in a glow discharge being set up in the gas, and a Xe dimer vacuum UV (VUV) emission predominantly between 147 and 190 nm occurs. (In comparison, the mercury discharge in a conventional fluorescent tube emits primarily at 254 nm.) The UV discharge excites red, blue, or green phosphors coated on one of the cells; each colour is activated by an adjacent electrode. The requirements for efficient output from these phosphors differ from conventional tubes since the latter were chosen on the basis of their luminescence efficiency at a 254-nm pump wavelength, and their resistance to degradation by the UV light and chemical attack by Hg^+ ions. These requirements are evidently different for the PDP technology; in addition the phosphors must have a significant reflection coefficient in the visible to optimise the light output [40.23], and the surface quality is of greater significance due to the short penetration depth of the VUV. The phosphors which have been used so far include $\text{BaMgAl}_{10}\text{O}_{17}:\text{Eu}^{2+}$ (blue), $\text{Zn}_2\text{SiO}_4:\text{Mn}^{2+}$ (green), and $(\text{Y}, \text{Gd})\text{BO}_3:\text{Eu}^{3+}$ and $\text{Y}_2\text{O}_3:\text{Eu}^{3+}$ (red). The blue phosphor is prone to degradation.

The widespread introduction of Xe excimer excitation in PDPs can be expected to stimulate applications in other lighting technologies. In this regard, the possibility of so-called *quantum cutting* is of much interest. This recognises that the energy of a VUV photon is equivalent to two or more visible photons, so that quantum efficiencies in excess of 100% can in principle be achieved. The difficulty lies in finding a luminescent ion system whose energy-level system provides for both efficient pumping and two-photon luminescence in the visible. One

example which has been reported to have a quantum efficiency of up to $\approx 145\%$ is Pr^{3+} in YF_3 and other hosts [40.24, 25], where the excitation is through the allowed $4f^2 \rightarrow 4f^1 5d^1$ or host transitions. The system then decays to the $^1\text{S}_0$ excited state of the $4f^2$ configuration from which two-photon decay is possible through successive $^1\text{S}_0 \rightarrow ^1\text{I}_6$ and $^3\text{P}_0 \rightarrow ^3\text{H}_j, ^3\text{F}_j$ transitions, as shown in Fig. 40.2. (The intermediate step from $^1\text{I}_6$ to $^3\text{P}_0$ is provided by a nonradiative transition.) A difficulty is that the photon for the first transition is in the UV region of the spectrum, and so it is necessary to incorporate a second luminescent ion pumped by this transition to convert the UV to visible output, and the visible quantum efficiency is necessarily reduced.

40.6.5 Scintillators

Although semiconductor detectors of ionising radiation are making increasing inroads into the particle detection market, traditional scintillators are still widely used and are indispensable for some applications. The operating principle is that an incident gamma ray creates a large number of electron–hole pairs in the scintillating material directly or indirectly through the photoelectric effect, Compton scattering, or pair production, and that some of the energy of recombination appears as photon emission from luminescent ions. Charged particles such as protons produce electron–hole pairs through the Coulomb interaction with the band electrons. The *scintillation* or multiphoton bursts which signal the event is detected by a photomultiplier, and the height of the output pulse from the photomultiplier is proportional to the energy of the particle. A pulse-height analyser sorts the pulses according to energy, and so an energy spectrum can be obtained. Key figures of merit for a scintillator material are the numbers of photons per MeV of particle energy, the radiative lifetime of the luminescent ion (since possible pulse overlap limits the maximum count rate which can be measured), and the weighted density ρZ_{eff}^4 , which reflects the gamma sensitivity. (Here Z_{eff} is the effective atomic number.) A recent review of scintillators has been given by *van Eijk* [40.26]. The most widely used scintillator for many years has been $\text{NaI}:\text{Tl}$, but many different scintillators are being investigated, driven by the need for improved performance and lower cost for medical applications such as positron emission tomography (PET) and single-photon emission computed tomography (SPECT), and for large-scale elementary-particle facilities such as those at the Centre Européen pour la Recherche Nucléaire (CERN). In the latter regard, the Crystal Clear collaborative project and other programs

have resulted in several new materials such as LaBr_3 , LaCl_3 , Lu_2SiO_5 , Gd_2SiO_5 , and LuAlO_3 , all Ce-doped, and undoped $\text{Bi}_4\text{Ge}_3\text{O}_{12}$ and PbWO_4 , with typical performance figures of 10 000–50 000 photons/MeV and lifetimes of 10–50 ns. For gamma spectroscopy the pulse-height resolution is critical and $\text{LaBr}_3:\text{Ce}$ has twice the resolution of NaI:Tl . The fastest scintillators

are based on core-valence luminescence where a hole created in a core level recombines with an electron in the valence band. For example, BaF_2 shows this *cross-luminescence* effect with a lifetime as short as 600 ps. The effect is only shown by materials with a core-valence (CV) band energy gap less than the usual band gap, otherwise CV luminescence is absorbed.

40.7 Representative Phosphors

To conclude, we present in Table 40.2 a list of several luminescent materials of practical significance. The table is intended to be representative rather than comprehensive.

It is noticeable from the table that just a few ions are responsible for a large number of applications, and primarily as oxides.

Table 40.2 Some luminescent materials of practical significance

Host	Dopants	Colour	Excitation	Application
$\text{Bi}_4\text{Ge}_3\text{O}_{12}$	–	Blue	Ionising radiation	Scintillator
ZnS	Ag^+	Blue	Electrons	Colour TV screens
$\text{Zn}_{0.68}\text{Cd}_{0.32}\text{S}$	Ag^+	Green	Electrons	Colour TV screens
$\text{Y}_3\text{Al}_5\text{O}_{12}$	Ce^{3+}	Yellow	Blue, violet	White LED
Gd_2SiO_5	Ce^{3+}	UV	Ionising radiation	Scintillator
ZnS	Cu^+	Green	Electrons	Colour TV screens
BaFBr	Eu^{2+}	UV/blue	X-rays	X-ray imaging
$\text{BaMgAl}_{10}\text{O}_{17}$	Eu^{2+}	Blue	UV	fluorescent lamps, plasma displays
Sr_3SiO_5	Eu^{2+}	Blue	UV	White LED
SrGa_2S_4	Eu^{2+}	Green	UV	White LED
SrAl_2O_4	Eu^{2+} , Dy^{3+}	Green	UV, violet	Persistent phosphor
CaAl_2O_4	Eu^{2+} , Nd^{3+}	Blue	UV, violet	Persistent phosphor
Y_2O_3	Eu^{3+}	Red	Electrons, UV	Colour TV screens, fluorescent lamps
Sr_2SiO_4	Eu^{3+}	Yellow	UV	White LED
$(\text{Y}, \text{Gd})\text{BO}_3$	Eu^{3+}	Red	UV	Plasma displays
Y_2O_3	Eu^{3+}	Red	UV	Plasma displays
SrY_2S_4	Eu^{3+}	Red	UV	White LED
LiF	Mg^{2+} and Ti^{4+}	UV/blue	Ionizing radiation	TL dosimetry
ZnS	Mn^{2+}	Yellow	Electric field	Panel displays
Zn_2SiO_4	Mn^{2+}	Green	UV	Plasma displays
$\text{CeMgAl}_{11}\text{O}_{19}$	Tb^{3+}	Green	UV	Fluorescent lamps

References

- 40.1 D. J. Vij: *Luminescence of Solids* (Plenum, New York 1998)
- 40.2 G. Blasse, B. C. Grabmeier: *Luminescent Materials* (Springer, Berlin, Heidelberg 1994)
- 40.3 G. H. Dieke: *Spectra and Energy Levels of Rare Earth Ions in Crystals* (Interscience, New York 1968)
- 40.4 W. T. Carnall, G. L. Goodman, K. Rajnak, R. S. Rana: *J. Chem. Phys.* **90**, 343 (1989)

- 40.5 E. Merzbacher: *Quantum Mechanics* (Wiley, New York 1970)
- 40.6 D. Curie: *Luminescence in Crystals* (Methuen, London 1962)
- 40.7 S. W. S. McKeever: *Thermoluminescence of Solids* (Cambridge Univ. Press, Cambridge 1985)
- 40.8 G. Kitis, J. M. Gomez-Ros, J. W. N. Tuyn: *J. Phys. D.* **31**, 2636–2641 (1998)
- 40.9 L. Botter-Jensen, S. W. S. McKeever, A. G. Wintle: *Optically Stimulated Luminescence Dosimetry* (Elsevier, Amsterdam 2003)
- 40.10 J. K. Park, C. H. Kim, H. D. Park, S. Y. Choi: *Appl. Phys. Lett.* **84**, 1647–1649 (2004)
- 40.11 S. Ken, O. Koji, K. Naoki, O. Masakazu, T. Daiichiro, H. Naoto, Y. Yominobu, X. Rong-Jun, S. Takayuki: *Opt. Lett.* **29**, 2001–2003 (2004)
- 40.12 P. L. Kim, P. E. Jeon, Y. H. Park, J. C. Choi, L. P. Park: *Appl. Phys. Lett.* **85**, 3696–3698 (2004)
- 40.13 D. Jia, R. S. Meltzer, W. M. Yen: *Appl. Phys. Lett.* **80**, 1535–1537 (2002)
- 40.14 D. Jia, X. J. Wang, E. van der Kolk, W. M. Yen: *Opt. Commun.* **204**, 247–251 (2002)
- 40.15 T. Aitasalo, A. Durygin, J. Holsa, J. Niittykoski, A. Suchocki: *J. Alloys Comp.* **380**, 4–8 (2004)
- 40.16 S. Schweizer: *Phys. Status Solidi* **187**, 335–393 (2001)
- 40.17 J. A. Rowlands: *Phys. Med. Biol.* **47**, R123–R166 (2002)
- 40.18 P. Hackenschmied, G. Schierning, A. Batentschuk, A. Winnacker: *J. Appl. Phys.* **93**, 5109–5113 (2003)
- 40.19 S. Schweizer, L. Hobbs, M. Secu, J.-M. Spaeth, A. Edgar, G. V. M. Williams: *Appl. Phys. Lett.* **83**, 449–451 (2003)
- 40.20 M. Secu, S. Schweizer, A. Edgar, G. V. M. Williams, U. Rieser: *J. Phys. C: Condens. Matter* **15**, 1–12 (2003)
- 40.21 A. Edgar, G. V. M. Williams, S. Schweizer, M. Secu, J.-M. Spaeth: *Curr. Appl. Phys.* **4**, 193–196 (2004)
- 40.22 J. P. Boeuf: *J. Phys. D* **36**, R53–R79 (2003)
- 40.23 H. Bechtel, T. Juestel, H. Glaeser, D. U. Wiechert: *J. Soc. Inform. Display* **10**, 63–67 (2002)
- 40.24 S. Kuck, I. Sokolska, M. Henke, M. Doring, T. Schefler: *J. Lumin.* **102–103**, 176–181 (2003)
- 40.25 A. B. Vink, P. Dorenbos, C. W. E. Van Eijk: *J. Solid State Chem.* **171**, 308–312 (2003)
- 40.26 C. W. E. Van Eijk: *Nuclear Instruments and Methods in Physics Research A* **460**, 1–14 (2001)